We are IntechOpen,
the world's leading publisher of
Open Access books
Built by scientists, for scientists

6,900
Open access books available

186,000
International authors and editors

200M
Downloads

154
Countries delivered to

Our authors are among the

TOP 1%
most cited scientists

12.2%
Contributors from top 500 universities

CLARIVATE ANALYTICS

BOOK CITATION INDEX

INDEXED

WEB OF SCIENCE™

Selection of our books indexed in the Book Citation Index
in Web of Science™ Core Collection (BKCI)

Interested in publishing with us?
Contact book.department@intechopen.com

Numbers displayed above are based on latest data collected.
For more information visit www.intechopen.com

Mathematical Description of Bayesian Algorithm for Speckle Reduction in Synthetic Aperture Radar Data

Daniela Colțuc

Additional information is available at the end of the chapter

1. Introduction

In remote sensing applications, the Synthetic Aperture Radar (SAR) images constitute a distinct class. The main particularity of this class is the image radiometry, which is a product between two signals: the terrain radar reflectivity R and the speckle s. The reflectivity depends on the terrain nature while the speckle is the consequence of the surface roughness. The speckle phenomenon is intrinsic to the radar technique. The radar sensor sends a coherent fascicle of microwaves toward the ground, which is scattered at the contact with the surface. The SAR antenna receives a non-coherent radiation resulted by the superposition of the reflected microwaves. These microwaves have random phase because of the surface roughness. The result is an image with a noisy aspect even in the regions with constant radar reflectivity. An example is the image in Figure 1, which represents a town surrounded by cultivated fields in French Guyana.
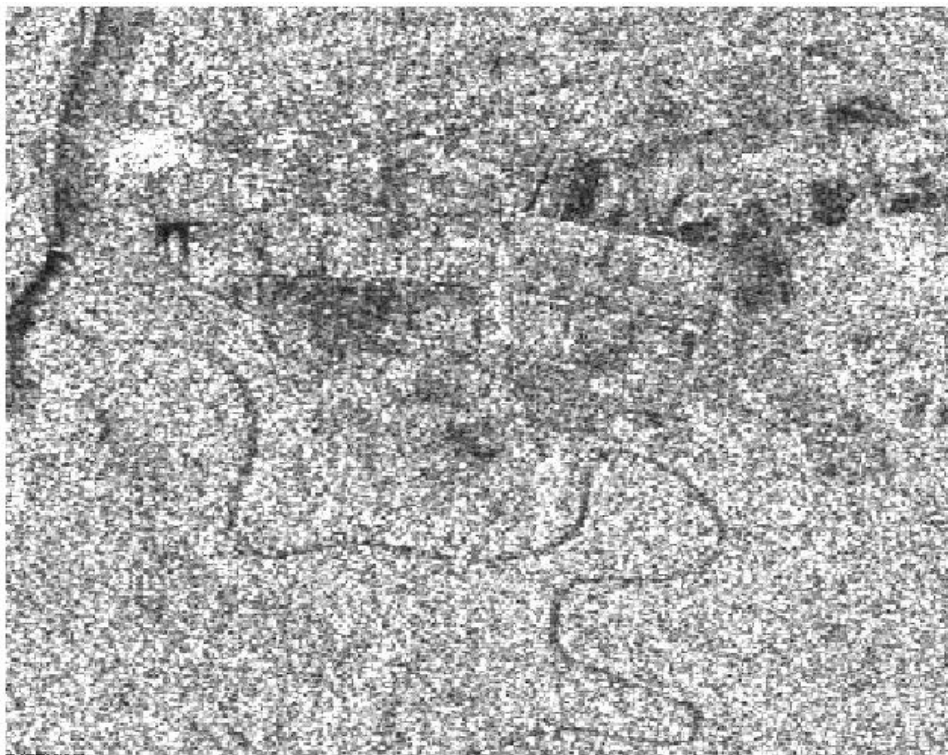
Although the speckle is carrying information that can be used in a series of applications, there are many cases where only R is of interest. In these situations, the speckle must be reduced in order to fully exploit the information in R.

The methods used to extract the reflectivity R from the SAR signal are known under the name of scene *reconstruction filters*. Among them, some of the most accurate in reconstruction are the Bayesian filters. These filters are based on the estimation theory, which has found a fertile terrain in SAR imagery due to the existing models for speckle. In the next section, we give a short overview of speckle distribution models in SAR imagery.

The Bayesian filters for speckle reduction were developed first for single SAR images and then extended to the multi-channel case. Here, the Bayesian filters have gained in efficiency due to the enhanced statistical diversity of the 3D data. This chapter presents several solutions for the

particular class of SAR multi-temporal series, which are sets of images of the same scene sensed at different dates. The rather long delays between acquisitions give the following special properties to these data: inter-channel speckle independency and radar reflectivity variation across the channels. The filters for multi-temporal SAR images presented in this chapter are either existing solutions, which were adapted to the above mentioned properties, or new approaches designed for the exclusive use on these data.

The multi-temporal SAR data have been used in a series of applications like change detection or land cover classification. While the majority of developed methods use a spatial speckle filtering as a pre-processing step [1-8], the recent publications have started reporting the use of multi-temporal filters [9-12].

Figure 1. Intensity SAR image.

The chapter begins with a brief description of speckle models, continues with the basics of estimation theory necessary to understand the Bayesian filters, presents some Bayesian filters for speckle reduction in single channel SAR images and ends with the solutions for speckle suppression in multi-temporal sets. At the end, we give some conclusions.

2. Speckle models in SAR images

The SAR images are of various types: complex, intensity, amplitude, logarithm, single-look and multi-looks. At the origin, it is the complex image that undergoes operations like pixels

modulus calculation (amplitude image), the square of modulus (intensity image), the logarithm of intensity (logarithm image) or the more complex multi-look processing consisting in pixels averaging and resampling.

In the complex SAR image, the pixels have complex values. The real part is the in-phase component of the measured radiation (same phase with the reference radiation of SAR sensor) and the imaginary part is the quadrature component.

In the case of fully developed speckle, both components have a Gaussian distribution:

$$P(z_1 \mid R) = \frac{1}{\sqrt{\pi R}} \exp\left(-\frac{z_1^2}{R}\right) \tag{1}$$

$$P(z_2 \mid R) = \frac{1}{\sqrt{\pi R}} \exp\left(-\frac{z_2^2}{R}\right) \tag{2}$$

where P is the probability density function (pdf), z_1 is the real part and z_2 the imaginary part. The eq. 1 and 2 show that, in a zone with constant reflectivity, the image pixels are varying because of speckle. By making $R = 1$, one obtains the speckle pdf in complex SAR images.

The SAR intensity image I is obtained from the complex image by considering the square of the modulus:
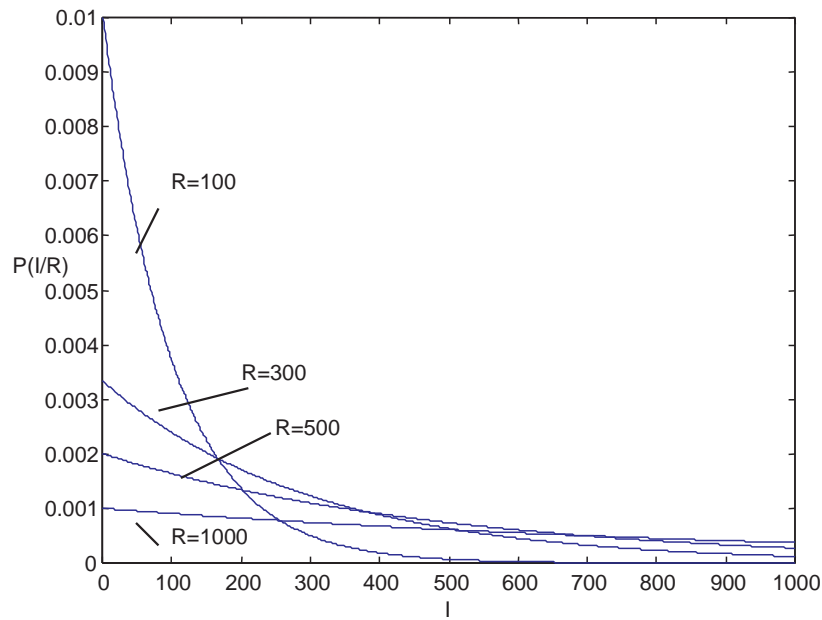
$$I = z_1^2 + z_2^2 \tag{3}$$

Generally, any mathematical operation with random variables (r.v.) changes the r.v. pdf. In the case of intensity images, the speckle pdf changes into an exponential distribution [13]:

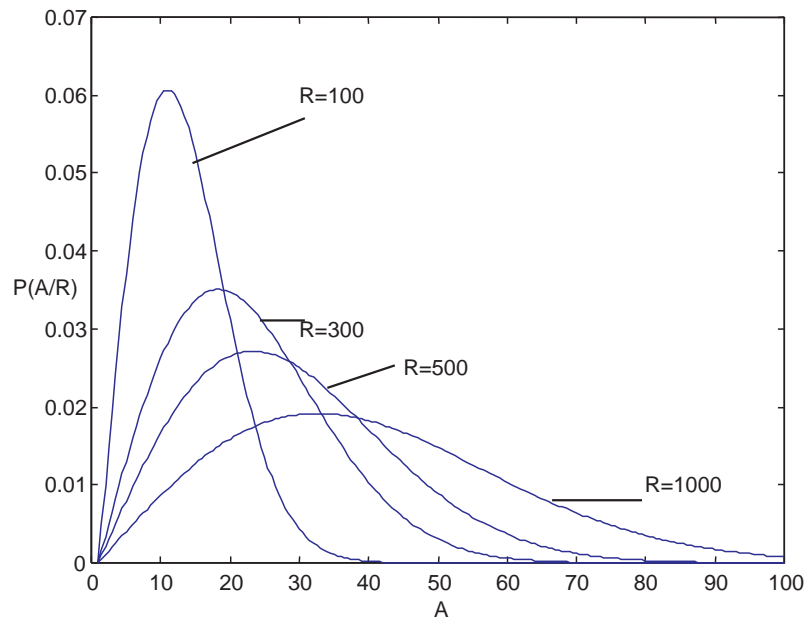$$P_I(I/R) = \frac{1}{R} \exp\left(-\frac{I}{R}\right) I \geq 0 \tag{4}$$

Fig. 2 shows the distribution in (4) for various values of R. The speckle distribution in SAR intensity images is obtained for $R = 1$.

The amplitude SAR image is the square root of the intensity image, $A = \sqrt{I}$ In this case, the speckle has a Rayleigh distribution (Fig. 3):

$$P_A(A/R) = \frac{2A}{R} \exp\left(-\frac{A^2}{R}\right) A \geq 0 \tag{5}$$

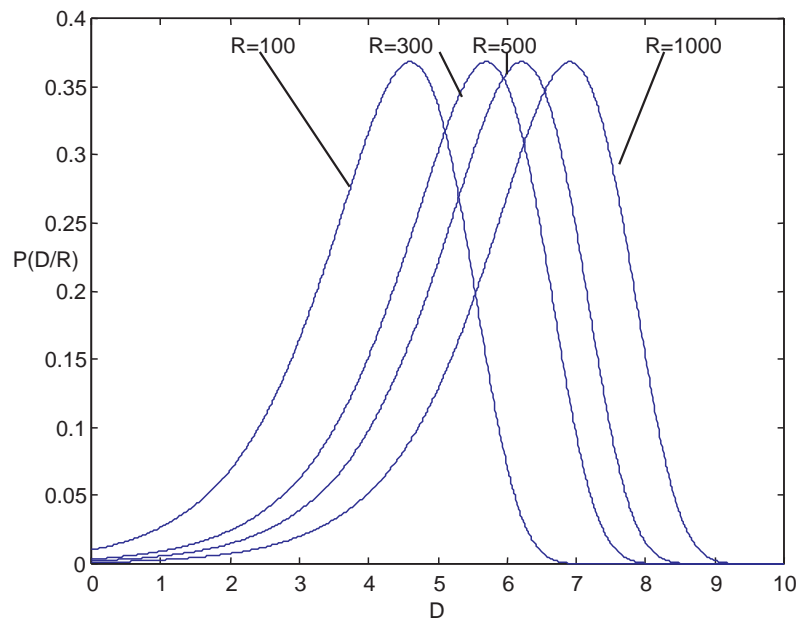**Figure 2.** Pixel pdf in an intensity image representing a zone with constant R.

Figure 3. Pixel pdf in an amplitude image representing a zone with constant R.

The curves in Fig. 2 and 3 show that, for both intensity and amplitude images, the pixels variance increases with R. This explains why the speckle, although stationary, appears as stronger in the light areas. It is, in fact, a consequence of the multiplicative nature of the speckle.

The logarithm image is the logarithm of the intensity $D=\ln(I)$. The logarithm image has a Fisher-Tippet distribution [14]:

$$P_D(D/R) = \frac{e^D}{R} \exp\left(-\frac{e^D}{R}\right) \tag{6}$$

For various R, the distribution changes its mean but not its variance (Fig. 4). Indeed, since the logarithm transforms any product into a sum, the speckle in the logarithm SAR image is an additive stationary noise, which explains the variance constancy.
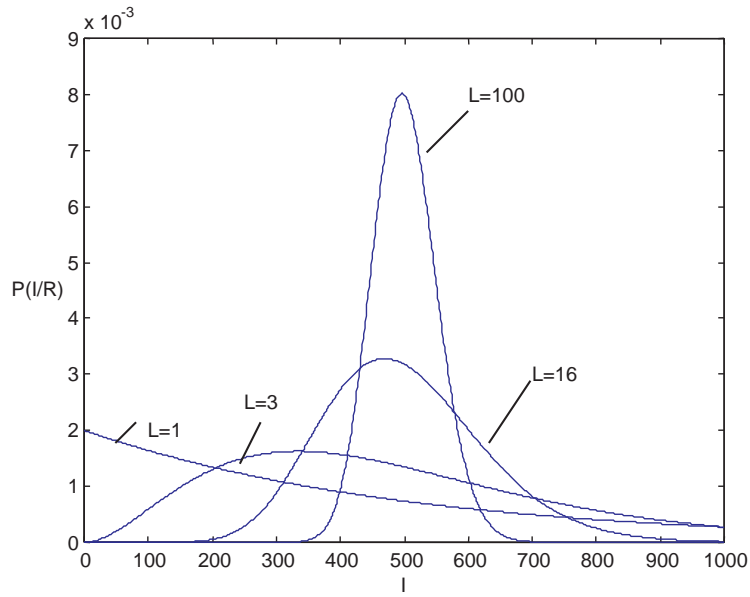

Figure 4. Pixel pdf in a logarithm image representing a zone with constant R.

The multi-look images are obtained by averaging, on columns, groups or 3 or 4 pixels. The resulting image must be interpolated and resampled in order to have the same resolution on rows and columns. Due to pixels averaging, the multi-look image is less noisy.

Depending on the image at the origin – intensity, amplitude or logarithm-the multi-look image can be of intensity, amplitude or logarithm type. The multi-look treatment changes the speckle distribution as follows:

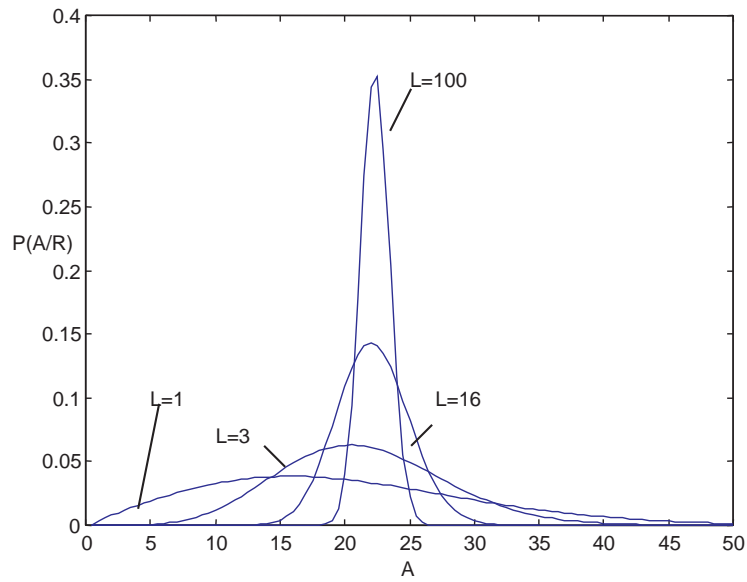• Gamma distribution in multi-look intensity SAR image [13] (Fig. 5):

$$P_I(I/R) = \frac{1}{\Gamma(L)}\left(\frac{L}{R}\right)^L I^{L-1} \exp\left(-\frac{LI}{R}\right) I \geq 0 \tag{7}$$

Figure 5. Pixel pdf in a multi-look intensity image representing a zone with constant R

where L is the number of looks (the number of averaged pixels).

- Generalized Gamma distribution in multi-look amplitude SAR image (Fig. 6):
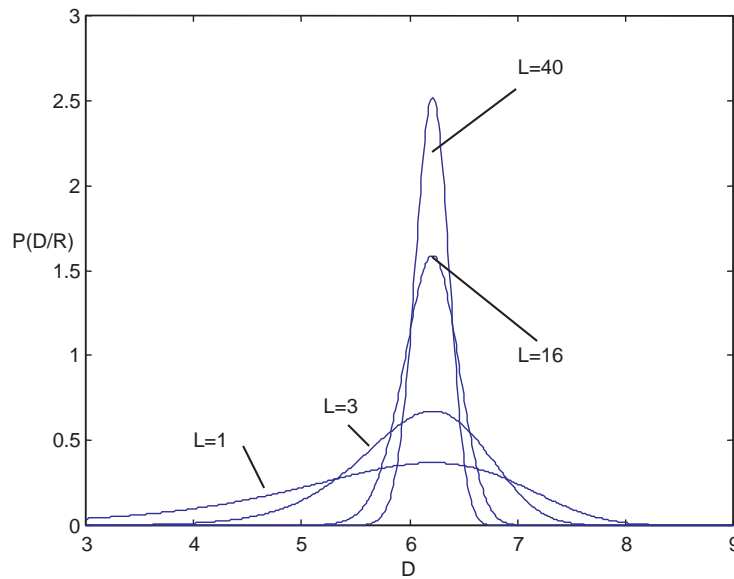

Figure 6. Pixel pdf in a multi-look amplitude image representing a zone with constant R.

$$P_A(A) = \frac{2}{\Gamma(L)} \left(\frac{L}{R}\right)^L A^{2L-1} \exp\left(\frac{-L A^2}{R}\right) A \geq 0 \qquad (8)$$

- Fisher-Tippet distribution in multi-look logarithm SAR images [13] (Fig. 7):

$$P_D(D\,\big|\,R) = \frac{L^{\,L}}{\Gamma(L\,)}\exp(-L\,(D_R-D))\exp(-L\,\exp(-(D_R-D)))$$

(9)

Figure 7. Pixel pdf in a multi-look logarithm image representing a zone with constant R.

where $D_R = \ln(R)$. As shown in Figures 5-7, in all the types of multi-look images, the speckle variance is reducing as the number of looks increases. The other side of the coin is the lower resolution of the resulted image.

Another aspect-important for Bayesian filters which are based on the calculus of estimates-is the speckle correlation. The speckle becomes a correlated signal at the sensor level that has a limited band. In estimation, the samples correlation worsens the estimate precision.

3. Basics of estimation theory

The multiplicative model $I = R \cdot s$ shows that the SAR image radiometry I can be interpreted as a random signal having the reflectivity R as parameter. The Estimation Theory provides the means to estimate this parameter from the image pixels. The starting point in any estimation is a cost function $C(\varepsilon)$ that has as argument the estimation error:
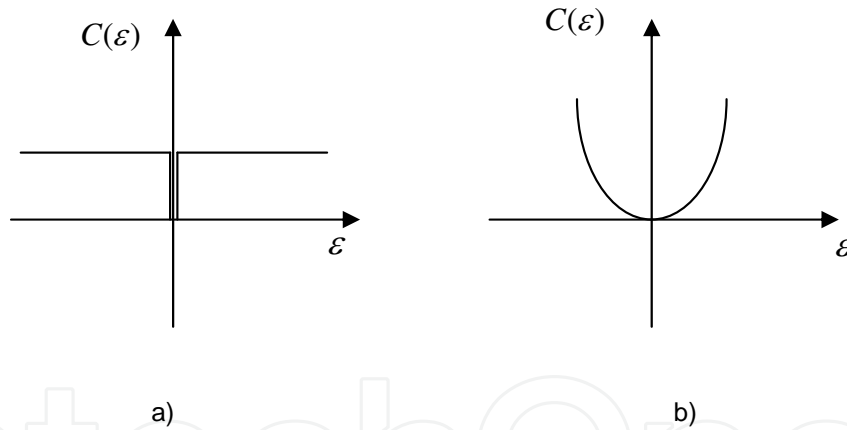
$$\varepsilon = \hat{R} - R$$

(10)

where $\hat{R}$ is the estimated value of the reflectivity and R its actual value. The cost measures the penalty introduced by the estimation error. Therefore, it is natural to estimate the reflectivity under the constraint of minimum cost. Since the cost is itself a random variable that cannot be known by its particular realizations but by its statistical moments, the condition for the estimator is to minimize the average cost:

$$\bar{C} = \iint C(\hat{R} - R) \cdot P(R,\ I)\, dR dI \tag{11}$$

where $P(R,\ I)$ is the joint pdf of R and I. The expression of $\hat{R}$ is found by solving the equation $\bar{C} = \min$.

The cost function can be defined in several ways. The most common ones are the uniform and the quadratic functions. The uniform cost function is equal to one everywhere, excepting the origin where it is equal to zero (Fig. 8a) :

$$C(\varepsilon) = 1 - \delta(\varepsilon) \tag{12}$$

Figure 8. Two cost functions: a) the uniform function, b) The quadratic function.

With this function the penalty is the same disregarding the estimation error. The quadratic function has a penalty that increases with the estimation error (Fig. 8b):

$$C(\varepsilon) = \varepsilon^2 \tag{13}$$

3.1. Estimators based on the uniform cost function

By introducing (12) in the average cost (11), one obtains the following equation:

$$\overline{C} = \iint [1 - \delta(\hat{R} - R)] P(R, I) dR dI =$$
$$= \iint P(R, I) dR dI - P(\hat{R}, I) = 1 - P(\hat{R}, I)$$

(14)

which means that, in the case of the uniform cost function, the estimate $\hat{R}$ is the value of the reflectivity that maximizes $P(\hat{R}, I)$. Since in many cases, $P(\hat{R}, I)$ has not an analytical expression or is too complex, it is replaced by $P(R, I) = P(R / I)P(I)$ and the estimate $\hat{R}$ is:

$$\max(P(R / I)) = P(\hat{R} / I)$$

(15)

This is the definition of the optimal estimator in the case of the uniform cost function. Since it is obtained by maximizing an a posteriori pdf, it is known as the *Maximum A Posteriori (MAP) estimator*. By using Bayes equation, $P(R / I)$ can be expressed as a function of $P(I / R)$, a distribution that is known in SAR imagery:

$$P(R \mid I) = \frac{P(I / R)P(R)}{P(I)}$$

(16)

According to (8), maximizing $P(R / I)$ is equivalent to maximizing $P(I / R)P(R)$ (the reflectivity does not appear explicitly in $P(I)$). When the reflectivity pdf $P(R)$ is not known, it can be considered constant (uniform distribution) and the estimate $\hat{R}$ is obtained by maximizing the a priori pdf:

$$\max(P(I / R)) = P(I / \hat{R})$$

(17)

The equation (9) defines *the maximum likelihood estimator* of $\hat{R}$, which is suboptimal by respect to MAP because it ignores the scene reflectivity distribution.

3.2. Estimators based on the quadratic cost function

The quadratic cost function gives an average cost of:

$$\overline{C} = \iint (\hat{R} - R)^2 \cdot P(R, I) dR dI$$

(18)

The minimization of $\overline{C}$ is equivalent to solving the equation:

$$\frac{d\overline{C}}{dR} = \iint 2(\hat{R} - R) \cdot P(R, I) dR dI =$$
$$= \int P(I) \left[\int 2(\hat{R} - R)P(R \mid I) dR \right] dI = 0$$

(19)

that gives the solution for the estimator $\hat{R}$:

$$\hat{R} = \int R \cdot P(R/I)dR = E[R/I] \tag{20}$$

The equation (20) shows that the optimal estimator, in the case of the quadratic cost function, is the conditional mean of the reflectivity. It can be derived from the SAR image radiometry if the a posteriori distribution $P(R/I)$ is known. When $P(R/I)$ is not known, a suboptimal estimate can be obtained by considering this distribution constant (uniform) and by using a linear estimate:

$$\hat{R} = ai + b \tag{21}$$

The coefficients a and b are obtained by minimizing the average cost, which in this particular case is:

$$\overline{C} = \iint (\hat{R} - R)^2 dRdI \tag{22}$$

4. Bayesian filters for single channel SAR images

4.1. Filters based on the quadratic cost function

a. Kuan Filter

The filter of Kuan is a linear estimator (21), based on the quadratic cost function. It is suboptimal because the a posteriori distribution $P(R/I)$ is considered uniform as in (22). Other simplifying hypotheses used in deriving this filter are the speckle and the radar reflectivity whiteness, which is not realistic in none of the cases. These hypotheses worsen the estimator quality but simplify a lot its analytical expression.

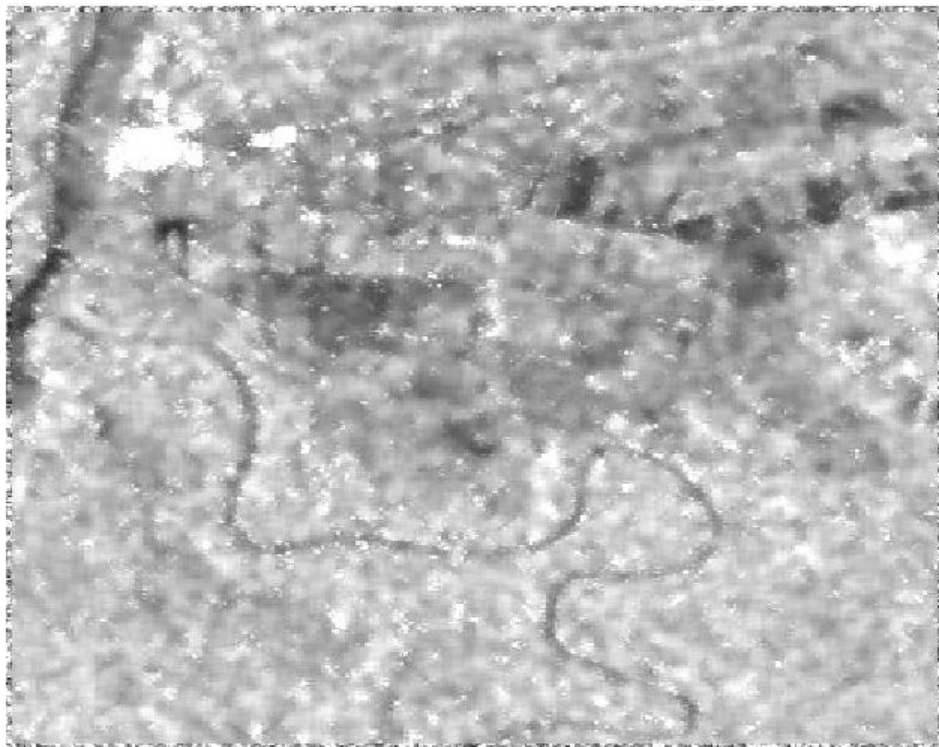The filter of Kuan estimates the radar reflectivity by [15]:

$$\hat{R}(x, y) = k \cdot I(x, y) + (1-k) \cdot \bar{I} \tag{23}$$

where $I(x, y)$ is the current pixel, $\bar{I}$ is the average radiometry in a window centered on $I(x, y)$ and k is a coefficient estimated in the same window. It is given by:

$$k = \frac{1 - c_s^2 / c_I^2}{1 + c_s^2} \tag{24}$$

where c_s and c_I are the speckle and the image coefficients of variation. The coefficient of variation is the ratio between the signal standard deviation and mean. For the speckle, it is known (it depends on SAR image type) and for the image, it is estimated locally.

The filter smoothes the image ($\hat{R}(x, y) = \bar{I}$) in the areas with constant reflectivity and favors the current pixel $I(x, y)$ on textured zones or edges. Figure 9 shows the result of filtering the SAR image in Figure 10, by Kuan filter. The coefficient of variation and the average intensity was estimated in a 9x9 neighborhood of the current pixel.

Figure 9. Scene reconstructed by Kuan filter with 9x9 neighborhoods.

b. Lee filter

The filter of Lee is of the same class as the filter of Kuan i.e., it is linear, based on the quadratic cost function and ignores the a posteriori distribution $P(R/I)$. The same hypotheses are considered: white speckle, white radar reflectivity and independence between speckle and reflectivity. The difference consists in the way it is derived. Being originally developed for additional noise, the speckle is first transformed into an additive noise by using the following approximation:

$$I(x, y) \approx A \cdot R(x, y) + B \cdot s(x, y) + C \tag{25}$$

Figure 10. Scene reconstructed by Lee filter with 9x9 neighborhoods.

where $A=\bar{s}$, $B=\bar{R}$, $C=-\bar{R}\cdot\bar{s}$ (the coefficients are determined from the conditions to have an unbiased estimator and a minimum average cost). By applying the Lee filter for additive noise on this approximation, Lee obtained the following estimator [16]:

$$\hat{R}(x,\,y)=\bar{I}+k(I(x,\,y)-\bar{I}) \quad \text{where} \quad k=1-\frac{c_s^2}{c_I^2} \tag{26}$$

Figure 4 shows the SAR image filtered by Lee filter using a 9x9 neighborhood. The equations of Lee and Kuan filters are very similar. The difference is in the expression of k, which in the case of Lee filter is supplementary divided by $1+c_s^2$. This number tends to 1 in multilook SAR images, showing that the two filters process similarly these data. It is not the case for single look images where $1+c_s^2=2$ and, consequently, Lee filter is less accurate.

c.   Frost filter

Although of the same class as Kuan filter – linear, minimizing the quadratic cost and ignoring the a priori distribution – the filter of Frost reduces better the speckle by modifying the hypothesis regarding the radar reflectivity. Differently from Lee and Kuan, Frost considers the reflectivity a correlated signal and uses for the correlation the exponential model:

$$\rho_R(d) = e^{-ad} \qquad (27)$$

where ρ_R is the reflectivity coefficient of correlation, a is a parameter depending on the scene content and d is the pixel lag. As a consequence, the filter of Lee takes into account not only the current pixel $I(x, y)$ but all the pixels in the neighborhood (usually a 3x3 neighborhood). The filter coefficients in the 1D case are [17]:

$$w(d) = K\alpha e^{-\alpha d} \quad \text{with} \ \alpha^2 = K'c_I^2 \qquad (28)$$

where K has the role to remove the estimator bias and K' is a constant that tunes the filtering effect. For images, the filter (28) it is applied on rows and columns.

Other filters based on the quadratic cost function are the EAP (Estimator a Posteriori) and the t-linear filter. The EAP minimizes the average cost in (18) not the simplified condition in (25), by considering a Gamma distribution for the radar reflectivity. It is more accurate than Kuan, Lee or Frost filters but it is time consuming.

4.2. Filters based on the uniform cost function

The a posteriori distribution (15), which gives the MAP estimator, includes the a priori distribution (known for SAR images) and the reflectivity distribution. Each model used for the reflectivity distribution gives another estimator. The higher the model complexity, the better is the estimator. In this section, we give the estimators for the following three models of radar reflectivity pdf: uniform correlated distribution, Gamma uncorrelated distribution, Gamma correlated distribution.

A uniform correlated distribution for the reflectivity gives the following distribution for the intensity of the SAR image:

$$P_{loc}(I \mid R) = \left(\frac{\alpha}{R}\right)^L \frac{I^{\alpha-1}}{\Gamma(\alpha)} \exp\left[-\frac{\alpha I}{R}\right] \qquad (29)$$

where R is the reflectivity of the current pixel, I is the intensity of any pixel in the 3x3 neighborhood of R and α is a shape parameter:

$$\alpha = \frac{1}{c_I^2} \qquad (30)$$

In the hypothesis of uncorrelated intensity, the maximization of the a posteriori probability gives the following expression for MAP estimator:

$$\hat{R}(x, y) = \bar{I} + k(I(x, y) - \bar{I}) \quad \text{with} \ k = \frac{1}{1 + 8\alpha / L} \qquad (31)$$

where L is the number of looks. Being derived by considering a uniform distribution for the reflectivity, (31) is in fact a maximum likelihood estimator. The parameter α is estimated in the 3x3 neighborhood of the current pixel and $\bar{I}$ in a larger neighborhood.

A better estimator is obtaining by introducing in MAP equation a non-uniform model for the radar reflectivity distribution. The non-uniform model currently used for the reflectivity is the Gamma distribution:

$$P(R) = \left(\frac{v}{E[R]}\right)^v \frac{R^{v-1}}{\Gamma(v)} \exp\left(-\frac{vR}{E[R]}\right) \tag{32}$$

where v is a shape parameter equal to $1/c_R^2$. Between v and α it is the following connection:

$$v = \frac{1 + 1/L}{1/\alpha - 1/L} \tag{33}$$

The reflectivity estimator in this case is:

$$\hat{R}(x, y) = \frac{1}{2v}\left(E[R](v - L - 1) + \sqrt{E[R]^2(v - L - 1) + 4vLI(x, y)E[R]}\right) \tag{34}$$

where $E[R]$ and v are estimated in a neighborhood of the current pixel. For the intensity SAR images, $E[R] = E[I]$.

The maximum likelihood estimator in (31) takes into account the radar reflectivity correlation but consider a uniform distribution while the estimator in (34) ignores the correlation and consider a reflectivity with Gamma distribution. A filter that uses both a correlated and a Gamma distribution model is the following estimator:

$$\hat{R}(x, y) = \frac{1}{2v}(E[R](v - L - 1 - 8\alpha) +$$
$$+ \sqrt{E[R]^2(v - L - 1 - 8\alpha) + 4v(LI(x, y) + 8\alpha E[I])E[R]}) \tag{35}$$

where $E[R]$, $E[I]$, v and α are estimated on the image, in a neighborhood of the current pixel. Like for the other two filters, v and α are estimated in a 3x3 window and and E[R] and E[I] in larger neighborhood (the neighborhood size is chosen usually between 7x7 and 11x11 pixels).

The list of the Bayesian filters does not end here. This section has presented only several of them, which are the most used. Other filters from this class can be found in [18-21]. At a more attentive analysis, one can see that all these filters have in common the following behavior: in the areas with constant reflectivity, the reflectivity is estimated by the local mean of the intensity. The filters differ by the solution proposed in the textured areas and on the edges.

5. Bayesian filters for multi-temporal SAR images

The multichannel SAR images are 3D volumes of data constituted by assembling several SAR images representing the same scene. The images are registered i.e., the corresponding pixels in different channels (images) represent the same resolution cell at the ground. The Bayesian filters for multichannel images are in principal the same as for single SAR images: MAP, maximum likelihood and the conditional mean. The differences concern the neighborhood used by the estimators and the speckle statistics properties, more precisely the inter-channel correlation.

None of the Bayesian filters reconstructs perfectly a scene. Generally, the filtering result is a tradeoff between speckle reducing and texture and edges blurring. An essential role in making this tradeoff has the size of the neighborhood used for estimating the statistical moments included in filter expression. In a large neighborhood, the estimation is theoretically more accurate but many fine details can be lost. The main advantage of multichannel filters is in the neighborhood used for estimating the statistical moments. The existence of a third dimension allows the neighborhood extension by preserving a reasonable size in the image plane. For a given precision of the estimation, scene details are better preserved when 3D neighborhoods are used.

In the image plane, the speckle is a correlated signal. In estimation, the samples correlation is a withdraw because, at a given statistical population size, the estimation precision is worse than if the samples were independent. In multi-temporal sets, due to the significant time leg between acquisitions, the speckle components in different channels are not correlated. Therefore, the neighborhood extension on the 3rd dimension improves a lot the result of Bayesian filters.

This section presents three Bayesian filters for multi-temporal sets: the linear filter [22,23] (the equivalent of Lee filter), the Time-Space filter [24-26] and the Multi-temporal Non-Local Mean [30]. Other filters from the same class can be find in [28, 29].

5.1. The linear filter for multi-temporal SAR images

In Section 3.2, it was shown that when the a posteriori distribution of the reflectivity is not known, a linear estimator (21) can be obtained by minimizing the average quadratic error (22). It is the solution that gives the filters of Kuan, Lee or Frost. In the case of multichannel SAR images, the linear estimator is a weighted sum of the corresponding pixels in all the channels [22]:

$$\hat{R}_i(x,\ y) = \sum_{j=1}^{N} \alpha_j^{(i)} I_j(x,\ y) \frac{E[I_i]}{E[I_j]} \quad i = 1,\ \ldots,\ N \tag{36}$$

where N is the number of channels and $\alpha_j^{(i)}$ is a set of coefficients that are determined from the following conditions:

$$\min\left(E\left[(\hat{R}_i - R_i)^2\right]\right) \tag{37}$$

$$\sum_{j=1}^{N} \alpha_j^{(i)} = 1 \quad \forall \quad i = 1, \cdots, N \tag{38}$$

The equations (37) are the condition for minimum cost and (38) the condition for unbiased estimators.

By using the linear estimator (36), Bruniquel derived a multi-temporal version of Lee filter (26). Additionally, he improved the filter hypotheses, by considering that the scene has also textures and not only homogenous zones like in the case of Lee's filter. For channels with identical textures, the conditions (37, 38) become [22]:

$$\begin{cases} \sum_{j=1}^{N} \alpha_j^{(n)} = 1 \\ \sum_{j=1}^{N} \alpha_j^{(n)}(\rho_{i,j}c_ic_j - \rho_{j,n}c_jc_n) = 0 \quad i = 1, \ldots, N \quad i \neq n \end{cases} \tag{39}$$

Where $\rho_{i,j}$ is the coefficient of correlation between the channels i and j and c_i is the coefficient of variation in the channel i.

In multi-temporal sets, with high probability, the textures change from a channel to another because of the delay between the acquisitions (months, seasons or years). For this reason, in a second essay, Bruniquel introduced the hypothesis of different textures and obtained the following equations for the two conditions [23]:

$$\begin{cases} \sum_{j=1}^{N} \alpha_j^{(n)} = 1 \\ \sum_{j=1}^{N} \alpha_j^{(n)}(\rho_{i,j}c_ic_j - \rho_{n,j}c_nc_j) = \rho_{n,i}^{(n)}c_nc_i - c_n^2 \quad \begin{cases} i = 1, \ldots, N \\ i \neq n \end{cases} \end{cases} \tag{40}$$

In this case, the inter-channel correlation is not anymore the speckle correlation i.e., zero but the correlation between textures.

This filter uses the most realistic hypotheses for multi-temporal images and consequently it arrives to reconstruct rather well the scenes. The filter withdraw is the high complexity: for each pixel in the scene, one has to solve the system (40).

5.2. The time-space filter

A Bayesian filter for multi-temporal SAR images, both efficient and of low complexity but which passed almost unobserved, is the Time-Space filter. This filter takes advantage of the fact that, across the channels, the reflectivity is correlated while the speckle is independent, which means that they have different frequency bands. In order to separate in frequency these

two signals, the authors consider the logarithm of the images and then apply a 1D Discrete Cosine Transform (DCT) only on the 3rd dimension of the set. Due to the above mentioned properties, the reflectivity energy accumulates in zero frequency coefficients while that of speckle remains uniformly distributed over all frequencies. By filtering only the non-zero frequency coefficients, it is possible to obtain a good quality for the reconstructed scene. The non-zero frequency planes are filtered by using the filter of Lee for additive noise and the reconstructed channels are obtained by inverse DCT and exponential calculation.

The scene reconstruction is done in 6 steps [24, 26]:

1. Let be $I_0, \ldots, I_{N-1}$ the N channels of the multi-temporal set. The first step consists in calculating the logarithm of the images:

$$I_n \;\Rightarrow\; G_n = \ln(I_n) = \ln(R) + \ln(s) \quad \forall\, n \in [0, \ldots, N-1] \tag{41}$$

For the pixels with value 0, a normalization is necessary: one can either consider that the logarithm is zero (the error is insignificant for an image on 16 bits) or add 1 to all the pixels before applying the logarithm.

2. A DCT is applied across the multi-temporal set. More precisely, the vector $G_{xy}(n)$ constituted by the pixels with the same position (x, y) in the channels is transformed:

$$G_{xy}(n) = \begin{bmatrix} \ln I_0(x,\, y) \\ \cdots \\ \ln I_{N-1}(x,\, y) \end{bmatrix} \;\Rightarrow\; T_{xy}(k) = DCT\{G_{xy}(n)\} = \begin{bmatrix} T_0(x,\, y) \\ \cdots \\ T_{N-1}(x,\, y) \end{bmatrix} \tag{42}$$
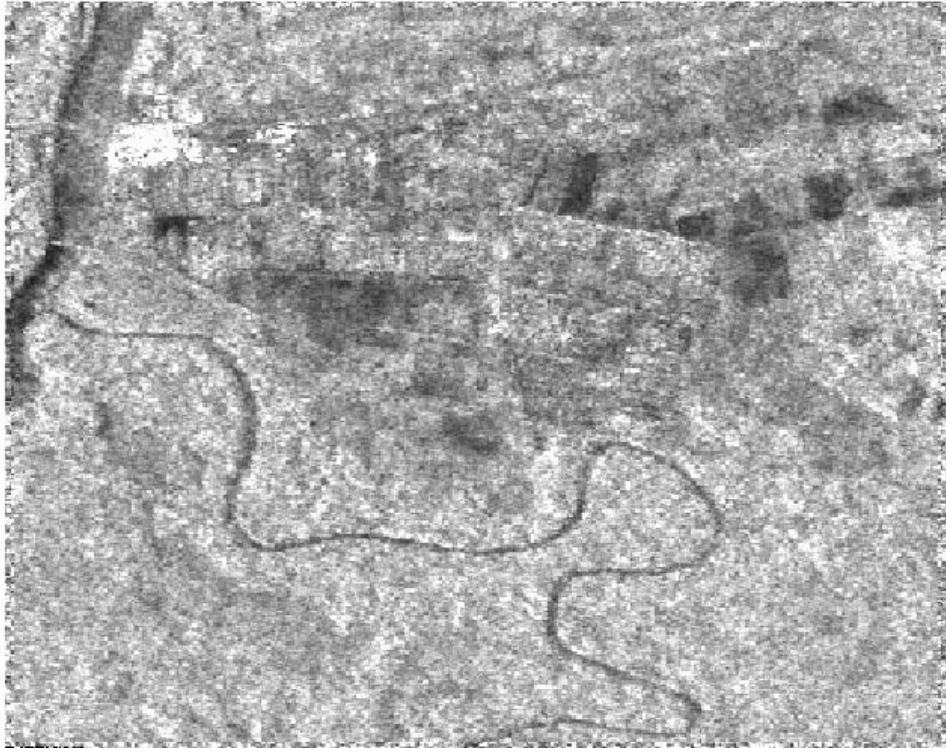
The result is a multispectral set with the same size as the multi-temporal set. The images are now constituted by DCT coefficients of the same frequency.

3. After DCT, the radar reflectivity, which is a correlated signal, is concentrated in $T(0)$. For this reason, $T(0)$ is conserved and only the rest of the frequency planes are filtered by using Lee's filter for additive noise:

$$\hat{T}_{xy} = E[T_{xy}] + (T_{xy} - E[T_{xy}]) \frac{\sigma_T^2 - \sigma_{zgomot}^2}{\sigma_T^2} \tag{43}$$

where the mean $E[T_{xy}]$ and the variance σ_T^2 are estimated in a neighborhood of (x, y). The variance σ_{zgomot}^2 is a parameter that depends on speckle statistics. It was shown that it can be approximated by the speckle coefficient of variation.

4. Inverse DCT of the filtered set:

Figure 11. Scene reconstructed by Time-Space Filtering of 6 multi-temporal SAR images.

$$\hat{T}_{xy}(k)=\begin{bmatrix} T_0(x,\ y) \\ \hat{T}_1(x,\ y) \\ ... \\ \hat{T}_{N-1}(x,\ y) \end{bmatrix} \quad \Rightarrow \quad \hat{G}_{xy}(n)=DCT^{-1}\{\hat{T}_{xy}(k)\}=\begin{bmatrix} \hat{G}_0(x,\ y) \\ \hat{G}_1(x,\ y) \\ ... \\ \hat{G}_{N-1}(x,\ y) \end{bmatrix} \tag{44}$$

5. The genuine dynamic range of the set is obtained by calculating the exponential:

$$\hat{G}_n \quad \Rightarrow \quad \hat{I}_n=\exp(\hat{G}_n) \quad \forall\, n \in [0,\ ...,\ N-1] \tag{45}$$

6. $\hat{I}_n$ is a biased estimator because of the logarithm in the first stage. In [25], it was shown that bias is a multiplicative constant that depends on SAR image type and on the number of channels:

$$bias=\left(\int_0^\infty s^{\frac{1}{N}} P(s)ds\right)^N \tag{46}$$

where $P(s)$ is the speckle pdf. The bias is corrected by:

$$\hat{I}_n \quad \Rightarrow \quad \hat{I}_n^{corect} = \frac{\hat{I}_n}{bias} \quad \forall \, n \in [0, \, \ldots, \, N-1] \tag{47}$$

Figure 11 shows the scene in Figure 1 reconstructed by applying the Time-Space filter on a set of 6 multi-temporal SAR images. The filter of Lee uses a neighborhood of 11x11 pixels for moments estimation. A smaller neighborhood (9x9 pixels) is used for single SAR image filtering in Figures 3 and 4. Obviously, the image in Figures 6 has the details much better preserved then in the case of single channel filtering, where an effect of watercolor dominates. Even the finest details in the field at the right side of the image are preserved.

5.3. Two steps multi-temporal Non-Local Means

The Non-Local Means (NLM) is a denoising technique, which estimates each pixel by a weighted average of the similar pixels. NLM is a weighted maximum likelihood estimator. The NLM weights are defined according to the distance between the similar pixels neighborhoods.

The NLM derived for SAR images in [27] uses weights refined iteratively:

$$\hat{R}(i) = \sum_{j \in W} w(i, \, j) I(j) \tag{48}$$

where $I(j)$ are the image pixels (indexed), $w(i, \, j)$ the weights and W is the search neighborhood. The weights are given by:

$$w(i, \, j) = \frac{1}{Z} \exp\left[-\frac{1}{h_0} S(i, \, j) - \frac{L}{h_1} R^{m-1}(i, \, j) \right] \tag{49}$$

with

$$S(i, \, j) = \sum \log\left[\frac{I(i, \, k) + I(j, \, k)}{I(i, \, k)^{1/2} I(j, \, k)^{1/2}} \right] \tag{50}$$

$$R^{m-1}(i, \, j) = \sum_{k \in K} \frac{[\hat{R}^{m-1}(i, \, k) - \hat{R}^{m-1}(j, \, k)]^2}{\hat{R}^{m-1}(i, \, k) \hat{R}^{m-1}(j, \, k)} \tag{51}$$

where Z is a normalization parameter, h_0 and h_1 control the decay of the weights, K is a patch with pixel i (or j) as center and $I(i, \, k)$ is the k-th neighbor of $I(i)$ in K.

The multi-temporal version of the iterated NLM for SAR images is a two steps algorithm [30]:

Step 1. Each channel is filtered by iterative NLM. Let be $\hat{R}_1, \, \ldots, \, \hat{R}_N$ the filtered channels. An improved image of a certain channel I_n is obtained by combining stable pixels in time while

keeping unchanged the pixels not in accordance with the other dates. This is done by deriving a binary mask for each couple $(\hat{R}_n, \hat{R}_m)$:

$$P_i(n, m) = \begin{cases} 1 & if \quad \dfrac{[\hat{R}_n(i) - \hat{R}_m(i)]^2}{R_n(i)R_m(i)} > T \\ 0 & otherwise \end{cases} \tag{52}$$

where T is a threshold. The improved channel is the weighted average:

$$I_n^{improved} = I_n + \sum_m P(n, m)\hat{R}_m \tag{53}$$

Step 2. The improved channel is filtered by the iterated NLM. Denoising on the temporally weighted average image $I_n^{improved}$ is comparable to (48). However, the pixels may have different (equivalent) number of looks depending on the number of averaged data. In this case the similarity $S(i, j)$ between pixels has to be modified to take into account varying number of looks.

6. Conclusions

The Bayesian filters for SAR images are based on speckle statistics and, when possible, on scene distribution. The experiments have shown that none of the Bayesian filters arrives to reconstruct perfectly a scene. Generally, the result is a tradeoff between the speckle reduction and texture and edges fading out. A crucial factor is the quantity of a priori information included in the statistical models used by the Bayesian filters. A more complex model gives better chances in scene reconstruction but increases the computation time.

The single channel filters – Kuan, Lee and Frost – presented in Section 4.1 are all linear estimates optimizing the quadratic cost function. In the homogenous areas, they estimate the radar reflectivity in the same manner i.e., by calculating the mean of the pixels in the filtering window. The challenge is however represented by the edges and textures, where each filter gives another result. The best of them is Frost filter that includes in the statistical model the reflectivity correlation. The worst is Lee filter, which transforms the speckle into an additive noise by truncating a Taylor series.

The multi-temporal counterparts of the Bayesian filters improve the results but do not solve entirely the scene reconstruction problem. The reflectivity estimation is better due to the highest number of samples and mainly due to inter-channel speckle independence. Meantime, other specific problems arise, like the mixing of the features from different channels (in multi-temporal sets, the textures generally change from a channel to another because of the delays between acquisitions).

The filters for multi-temporal sets are using the same approaches as for single channel reconstruction. Additionally, they include in the statistical models the inter-channel characteristics i.e., speckle independency and variation of the radar reflectivity. This supplementary information contributes to the quality of the reconstruction result.

The filter for multi-temporal sets in Section 5.1 is a linear filter optimizing the quadratic cost function, like Kuan, Lee or Frost filters. Differently from these filters, the multi-temporal estimate is a linear combination of the corresponding pixels in all the channels. By introducing the hypothesis of variable textures, this filter arrives to reconstruct not only the homogenous zones but also the textured ones. The withdraw is however its high complexity.

The Time-Space filter is basically the filter of Lee applied in the space of DCT. TheTime-Space filter cleverness is the transformation solely on the temporal coordinate. As a consequence, the speckle, which is white, is uniformly spread in all the frequency planes while the radar reflectivity is concentrated in a single plane. By filtering all the planes excepting the one concentrating the reflectivity and by restoring the temporal channels by inverse DCT, the scene appears well reconstructed also in its fine details. For six 3-looks amplitude images, the Time-Space filter reconstructs the temporal channels with approximately 16 equivalent number of looks.

The multi-temporal NLM is a promising but not yet mature method. The NLM estimator, which gives good results in single image filtering, has definitely a higher potential in the context of multi-temporal sets. Some preliminary results on 6 six TerraSAR images show a good reconstruction of the fine details.

Author details

Daniela Colţuc

University Politehnica of Bucharest, Romania

References

[1] Waske B..and Braun, M. Classifier ensembles fo r land cover mapping using multi-temporal SAR imagery. ISPRS Journal of Photogrammetry and Remote S ensing. 2009; 64, 450–457.

[2] Wang D. et al. Applicat ion of multi-temporal ENVISAT ASAR d ata to agricultural area mapping in the Pearl River Delta. International Journal of Remote Sensing. 2010; 31, 1555–1572.

[3] Zhang Y. et al. Mapping paddy rice with multi-temporal ALOS PALSAR imagery in southeast China. International Journal of Remote Sensing. 2009; 30, 6301–6315.

[4]   Goodenough et al. Multitemporal evaluation with ASAR of Boreal forests. Proceedings of Geoscience and Remote Sensing Symposium IGARSS 2009, 12-17 July 2009, Seul, Correa.

[5]   Maged M, Mazlan H. and Farideh M. Object recognitions in RADARSAT-1 SAR data using fuzzy classification. International Journal of the Physical Sciences 2011; 6(16) 3933 – 3938.

[6]   Maged M. and Mazlan H. Developing adaptive algorithm for automatic detection of

[7]   al linear features using RADARSAT-1 SAR data. International Journal of the Physical Sciences 2010; 5(14), 2223-2229.

[8]   Maged M. RADARSAT for Oil Spill Trajectory Model. Environmental Modelling & Software 2004; (19), 473-483.

[9]   Maged, M. Radar Automatic Detection Algorithms for Coastal Oil Spills Pollution. International Journal of Applied Earth Observation and Geo-information 2001; (3)(2), 191-196.

[10] Yousif O. and Ban Y. Improving Urban Change Detection from Multitemporal SAR Images Using PCA-NLM. IEEE Tr. on Geoscience and Remote Sensing. 2013; 51(4) 2032 – 2041.

[11] Thiel C. et al. Analysis of multi-temporal land observation at C-band. Proceedings of Geoscience and Remote Sensing Symposium IGARSS 2000, 24-28 July 2000, Honolulu, Hawaii, USA.

[12] Satalino G. et al. Wheat crop mapping by using ASARAP data. IEEE Tr. on Geoscience and Remote Sensing. 2009; 47 527–530.

[13] Martinez, J.M. and Toan, T.L. Mapping of flood dynamics and spatial distribution of vegetation in the Amazon flood plain using multitemporal SAR data. Remote Sensing of Environment, 2007; 108, 209–223.

[14] Maître H. et al.Traitement des images de radar à synthèse d'ouverture. Hermes Science Europe Ltd. 2004.

[15] Oliver C. and Quegan S. Understanding Synthetic Aperture Radar Images with CDROM. SciTech Publishing; 2004.

[16] Kuan D et al. Adaptive restoration of images with speckle. IEEE Transactions on Acoustics, Speech and Signal Processing 1987; 35(3) 373-383.

[17] Lee J-S. et al. Speckle filtering of synthetic aperture radar images: A review. Remote Sensing Reviews 1994; 8(4) 313-340.

[18] Frost et al. A model for radar images and its implications to adaptive digital filtering of multiplicat ive noise. IEEE Transactionson Pattern Analysis and Machine Intelligence2009; 4, 157–166.

[19] Lopes. et al. Structure detection and statistical adaptive speckle filtering in SAR images. Int. J. Remote Sens.,1993; 14(9) 1735–1758, 1993.

[20] Yu Y. and Acton S.T. Speckle reducing anisotropic diffusion. IEEE Trans. Image Processing, 2002; 11(11) 1260–1270.

[21] Nicolas J.M., Tupin F. and Maitre H. Smoothing speckled SAR images by using maximum homogeneous region filters: An improved approach. Proceedings of Geoscience and Remote Sensing Symposium IGARSS'01, 9-13 July 2001, Sydney, Australia.

[22] Feng H., Hou B. and Gong M. SAR image despeckling based on local homogeneous-region segmentation by using pixel-relativity measurement. IEEE Trans. Geosci. Remote Sens. 2011; 49(7) 2724–2737.

[23] Bruniquel J. and Lopes A. Analysis and enhancement of multi-temporal SAR data.Satellite Remote Sensing. International Society for Optics and Photonics 1994; 342-353.

[24] Bruniquel J. and Lopes A. Multi-variate optimal speckle reduction in SAR imagery. International journal of remote sensing 1997 18(3) 603-627.

[25] Coltuc D. et al. Time-space filtering of multitemporal SAR images. Proceedings of Geoscience and Remote Sensing Symposium IGARSS 2000, 24-28 July 2000, Honolulu, Hawaii, USA.

[26] Coltuc D., Trouvé E. and Bolon Ph. Bias correction and speckle reduction in time-space filtering of multi-temporal SAR images. Proceedings of Geoscience and Remote Sensing Symposium IGARSS'01, 9-13 July 2001, Sydney, Australia.

[27] Coltuc D. and Radescu R. On the homomorphic filtering by channels' summation. Proceedings of Geoscience and Remote Sensing Symposium IGARSS'02, 24-28 July 2002, Toronto, Canada.

[28] Deledalle C-A., Denis L. and Tupin F. Iterative weighted maximum likelihood denoising with probabilistic patch-based weights. IEEE Transactions on Image Processing 2009;18(12) 2661-2672.

[29] Gineste P. A simple, efficient filter for mu lti-temporal SAR images. International Journal of Remote Sensing, 1999; 20, 2565–2576.

[30] Quegan S.and Yu J.J. Filtering of multichannel S AR images. IEEE Transactions on Geoscience and Remote Sensing, 2001; 39, 2373–2379.

[31] Su X. et al. Two steps multi-temporal non-local means for SAR images. Proceedings of Geoscience and Remote Sensing Symposium IGARSS 2012, 22-27 July 2012, Munich, Germany.